

Formation preference of divacancy ensemble in 4H-SiC

Ke Jing(靖克), Hui Qi(齐晖), Hangyu Liu(刘航宇), Feifei Zhou(周飞飞), Yunhong Zhao(赵云红), Bo Hong(洪波), Ying Dong(董莹), Jie Ma(马杰), Jiajun Li(李佳君), Hongwei Chen(陈宏伟), Xinqing Wang(王新庆)
Citation: Chin. Phys. B. 35, 096101 (2026). DOI: 10.1088/1674-1056/ae3e71 |
CSTR: 32038.14.CPB.ae3e71
http://cpb.iphy.ac.cn; http://iopscience.iop.org/cpb

What follows is a list of articles you may be interested in

Er intercalation and its impact on transport properties of epitaxial graphene

Mingmin Yang(杨明敏), Yong Duan(端勇), Wenxia Kong(孔雯霞), Jinzhe Zhang(章晋哲), Jianxin Wang(王剑心), Qun Cai(蔡群)
Chin. Phys. B. 32, 066103 (2023). DOI: 10.1088/1674-1056/acbc6a

Assessing the effect of hydrogen on the electronic properties of 4H-SiC

Yuanchao Huang(黄渊超), Rong Wang(王蓉), Yiqiang Zhang(张懿强), Deren Yang(杨德仁), Xiaodong Pi(皮孝东)
Chin. Phys. B. 31, 056108 (2022). DOI: 10.1088/1674-1056/ac4234

Theoretical study on the improvement of the doping efficiency of Al in 4H-SiC by co-doping group-IVB elements

Yuanchao Huang(黄渊超), Rong Wang(王蓉), Yixiao Qian(钱怡潇), Yiqiang Zhang(张懿强), Deren Yang(杨德仁), Xiaodong Pi(皮孝东)
Chin. Phys. B. 31, 046104 (2022). DOI: 10.1088/1674-1056/ac20ca

Influence of helium on the evolution of irradiation-induced defects in tungsten: An object kinetic Monte Carlo simulation

Peng-Wei Hou(侯鹏伟), Yu-Hao Li(李宇浩), Zhong-Zhu Li(李中柱), Li-Fang Wang(王丽芳), Xingyu Gao(高兴誉), Hong-Bo Zhou(周洪波), Haifeng Song(宋海峰), Guang-Hong Lu(吕广宏)
Chin. Phys. B. 30, 086108 (2021). DOI: 10.1088/1674-1056/abf7ac

Molecular dynamics simulations of cascade damage near the Y2Ti2O7 nanocluster/ferrite interface in nanostructured ferritic alloys

Yi-Qiang Sun(孙祎强), Wen-Sheng Lai(赖文生)
Chin. Phys. B. 26, 076106 (2017). DOI: 10.1088/1674-1056/26/7/076106

Formation preference of divacancy ensemble in 4H-SiC

Ke Jing(靖克)[1,3], Hui Qi(齐晖)[2], Hangyu Liu(刘航宇)[1], Feifei Zhou(周飞飞)[1], Yunhong Zhao(赵云红)[4], Bo Hong(洪波)[1], Ying Dong(董莹)[1], Jie Ma(马杰)[5], Jiajun Li(李佳君)[1,†], Hongwei Chen(陈宏伟)[1,‡], and Xinqing Wang(王新庆)[1]

[1] *College of Metrology Measurement and Instrument, China Jiliang University, Hangzhou* 310018, *China*

[2] *College of Materials and Chemistry, China Jiliang University, Hangzhou* 310018, *China*

[3] *Laboratory of Spin Magnetic Resonance, School of Physical Sciences, Anhui Province Key Laboratory of Scientific Instrument Development and Application, University of Science and Technology of China, Hefei* 230026, *China*

[4] *College of Civil Engineering and Architecture, Zhejiang University of Water Resources and Electric Power, Hangzhou* 310018, *China*

[5] *Key Laboratory of Artificial Structures and Quantum Control, School of Physics and Astronomy, Shanghai Jiao Tong University, Shanghai* 200240, *China*

(Received 19 November 2025; revised manuscript received 21 January 2026; accepted manuscript online 28 January 2026)

The divacancy ensemble in 4H silicon carbide (4H-SiC) is a promising spin-defect candidate for quantum sensing and scalable quantum technologies. The ability to fabricate well-defined divacancy ensembles is essential for practical implementation. In this work, the formation characteristics of divacancy ensembles are systematically investigated. First, a strong host dependence of divacancy formation is observed. The high purity semi-insulating (HPSI) 4H-SiC substrates yield high divacancy concentrations, followed by the epitaxial layer, whereas the formation is significantly suppressed both in the heavily doped n-type and p-type substrates. Second, the fabrication process exhibits remarkable selectivity among different divacancy configurations. The photoluminescence intensities of PL1 and PL2 centers dominate the ensemble in all suitable hosts among types of hosts with isochronal annealing comparison. The migration of silicon vacancy dominates the formation of divacancy, whose migration barrier is tuned by Fermi level. It also confirms that the electron irradiation and annealing process is a general routine to fabricate divacancy ensembles. Third, the PL5 ensemble is only observed in a specific host with various treatments. The formation of PL5 is strongly linked to the specific point defects with high formation barriers, rather than stacking faults, which makes it feasible to fabricate PL5 ensembles with uniform spatial distribution. Finally, magnetic response of PL1 ensemble is achieved at room temperature successfully. Its structural characteristics eliminate the need of additional bias magnetic field for resonant degeneracy. This work offers a new insight into defect engineering in wide-bandgap semiconductors. It also provides a reliable fabrication strategy for tailored divacancy ensembles in 4H-SiC and advances their potential for practical quantum sensing applications.

Keywords: divacancy ensemble, defects kinetics, quantum magnetometry, 4H-SiC

PACS: 61.72.Cc, 76.30.Mi, 07.55.Ge, 61.82.Fk

DOI: 10.1088/1674-1056/ae3e71 **CSTR:** 32038.14.CPB.ae3e71

1. Introduction

The controlled fabrication of color-center ensembles constitutes a fundamental prerequisite for practical quantum sensing applications.[1–3] Among the prominent defects in wide-bandgap semiconductors, divacancies in 4H type silicon carbide (4H-SiC) have attracted considerable attention since the demonstration of the room-temperature coherent spin properties.[4–6] These defects have enabled the successful detection of multiple physical quantities, including temperature, magnetic fields, and electric fields, highlighting their versatility in quantum metrology.[7–10] Furthermore, the mature 4H-SiC semiconductor industry provides a compelling pathway toward integrated and scalable quantum sensing platforms. Therefore, the reliable production of color-center ensembles represents an essential demand for advancing both fundamental research and practical quantum technologies.

Divacancies (labeled as PL1–PL4 with distinct lattice sites and PL5–PL8 with unidentified structures) constitute a class of intrinsic deep-level defects in 4H-SiC.[11,12] However, the high formation energies of divacancies make the species and concentrations difficult to control in as-grown wafers.[13,14] High purity semi-insulating (HPSI) wafers are preferred hosts for fabricating divacancies, yet the composition of the resulting ensembles varies across studies.[15–18] Conventional defect-engineering methods, such as electron irradiation and ion implantation, are widely employed to introduce divacancies, and the resulting defect distribution is strongly influenced by the specific fabrication process. For example, helium and carbon ion implantation have been reproduce divacancy ensembles and arrays near the surface of wafers, which preferentially produce PL4 along with the low yield of PL5 and PL6.[18–22] Electron irradiation is another method to fabricate ensembles. Some works reported the generation of PL1–PL4, whereas others observed no detectable

†Corresponding author. E-mail: lijiajun@cjlu.edu.cn

‡Corresponding author. E-mail: hwchen9814@cjlu.edu.cn

© 2026 Chinese Physical Society and IOP Publishing Ltd. All rights, including for text and data mining, AI training, and similar technologies, are reserved.

PL3.[23] Experimental discrepancies indicate a selective formation behavior among types of divacancies, suggesting that the mutually influential or restrictive factors govern the final formation of divacancy ensembles. The PL5 center in 4H-SiC has attracted considerable attention due to its outstanding room-temperature coherent properties.[24] The symmetry of PL5 has been proved to be C_{1h}, but its atomic configuration remains debated. For instance, Ivády *et al*. proposed that a quantum well induced by a stacking fault could stabilize the charge state of a divacancy, leading to the specific configuration of PL5.[25] Son *et al*. attributed PL5 to a slightly off-axis divacancy configuration based on the fine-structure parameter analysis of EPR.[26] More recently, Bai *et al*. suggested from the first-principles calculations that PL5 may correspond to an oxygen-vacancy complex.[27] To date, PL5 has been detected as a native defect in some HPSI wafers and can be fabricated with ion implantation and laser writing.[20,24,28] However, the formation kinetics of PL5 is unclear.

In this work, the formation preferences of divacancy ensembles have been discussed systematically across commonly used 4H-SiC wafers, which reveals a strong host dependence. Notably, PL1 and PL2 consistently dominate the ensemble composition regardless of the host types, indicating a pronounced type selectivity. It is proved that the depth distribution of divacancy ensembles is different in various hosts, following the distribution of silicon vacancies (V_{Si}, including the crystallographically distinct configurations of V_1' and V_2). Isochronal annealing results indicate that V_{Si} act as the key precursors for divacancy formation, while the production of electron irradiation is similar across types of hosts. Interestingly, the PL5 signal is exclusively detected in one specific HPSI host. Defect characterization indicates that the emergence of PL5 is linked to specific intrinsic defects acting as preferential precursors. Importantly, no stacking faults or dislocations are found along with divacancy ensembles with the fabrication processes, making it a gentle method for ensemble fabrication. Finally, the PL1 ensemble is applied to magnetic detection at room temperature successfully, demonstrating its immediate application and paving the way for practical quantum sensing devices based on 4H-SiC.

2. Materials and methods

The host wafers in this work were PVT substrates including HPSI (two wafers from different production batches, labeled as HPSI-1 and HPSI-2), n-type and p-type wafers, and one n-type epitaxial wafer (10 μm-thick on an n-type substrate). Detailed parameters are listed in Table S1. Electron irradiation was performed with a linear electron accelerator (10 MeV, CIAE-DZ-10/20). The electron beam was incident normally on samples with a fluence of 1×10^{18} cm^{-2}. Samples were cooled with a water-cooling stage during treatment, whose temperature was below 100 °C, monitored with an infrared thermometry. Samples were ultrasonically cleaned in anhydrous ethanol and deionized water for 10 min each, then annealed in a vacuum tube furnace with a base pressure of $< 5\times10^4$ Pa (OTF-1200X-S & GSL-1750X). Samples were heated from room temperature to 200 °C with a heating rate of 20 °C/min and held for 60 min to remove the possible absorbed moisture or gas, then they were heated from 200 °C to the annealing temperature with a heating rate of 20 °C/min, followed by a subsequent 30 min isothermal soak. Samples were cooled to room temperature naturally in the furnace. The pumping system worked during the whole annealing process.

Defect signals were analyzed with photoluminescence spectroscopy at 77 K (PL, 785 nm, alpha 300R, WITec & 325 nm, Lab RAM HR Evolution, Horiba) and electron paramagnetic resonance at 100 K (EPR, EMXplus-9.5/12, Bruker). The crystallographic structures were examined by high-resolution transmission electron microscopy (TEM, Talos F200 & Themis Z). The specimens for TEM were fabricated by the focused ion beam (FIB, Helios 5UX).

The optically detected magnetic resonance (ODMR) measurements were carried out with a home-built confocal setup. Ensembles were excited by a 914 nm laser (MIL-H-914-200 mW). The signal was collected with a microscope objective (M Plan Apo NIR 20X, Mitutoyo). Fluorescence and laser signals were separated by a dichromic beam splitter (DMLP1000, Thorlabs), filtered by a long-pass filter (FELH1000, Thorlabs), and coupled to a single-mode fiber to the photoreceiver (OE-200-IN1, Femto). The microwave signal was fed to a 40-μm copper wire across the surface of samples, which was generated with a signal generator (DSG 3065B, Rigol) and amplified with an amplifier (ZHL-5W-422+, Mini-circuits). A permanent magnet was positioned to provide a static magnetic field.

3. Results and discussion

The formation of divacancy ensembles was initially investigated with PL spectra at 77 K. All samples were irradiated with 10 MeV electrons at a fluence of 1×10^{18} cm^{-2} to create a high yield of vacancy precursors, followed by annealing at 1000 °C for 30 min to promote vacancy migration and divacancy formation.[29–32] PL spectra in the divacancy emission range were collected at 77 K, as shown in Fig. 1(a). For the HPSI and epitaxial hosts, characteristic divacancy peaks corresponding to PL1/2 (1132.0 nm/1130.5 nm), PL3 (1107.6 nm), PL4 (1078.5 nm) are clearly observed. The phonon side band (PSB) of PL1/2 is clear.[33,34] All divacancy peaks are superimposed on the PSB of V_{Si} (Fig. S1). In contrast, no discernible divacancy signals were obtained from the heavily doped n-type and p-type substrates under the present experimental conditions. There is a connection between the

formation of PL5 and the intrinsic property of HPSI-1. Given the overlapping of PL1 and PL2 peaks, Gaussian fitting was applied to deconvolute their contributions (Fig. S3). The concentration variation of divacancies is quantitatively compared with the integrated area of peaks across hosts under the same test conditions, as shown in Fig. 1(b). It shows that the intensity of each divacancy decreases in the order of HPSI-1, HPSI-2, epitaxial layer. PL1 and PL2 consistently dominate the divacancy ensemble across types of hosts. PL5 is exclusively detected in one specific HPSI host, which is strongly connected with the intrinsic property of HPSI-1. Notably, the PL5 emission (1141.9 nm) was exclusively detected in the HPSI-1 host.[35] The irradiation dose for HPSI-1 was reduced to match the divacancy intensity of HPSI-2, where PL5 is persistently detected in HPSI-1 even with the lowest irradiation dose (Fig. S2). Raising the irradiation dose also shows a positive effect on increasing the densities of PL1–PL4. Therefore, the possible concentration effect on the detector limitation or formation efficiency of PL5 is ruled out. These results show a strong host preference in the divacancy formation.

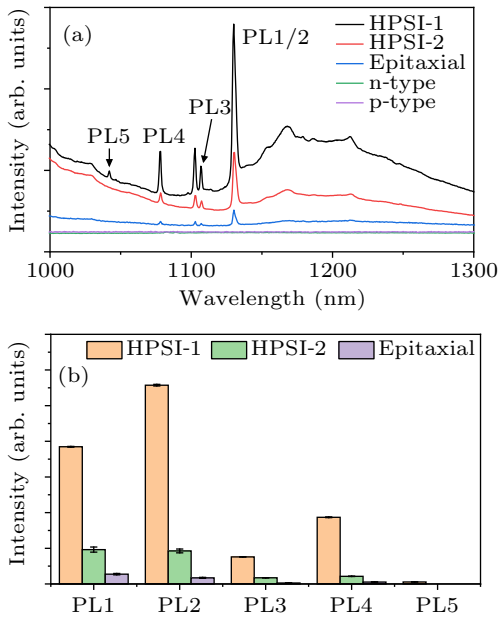


Fig. 1. (a) Photoluminescence spectra of divacancies in different 4H-SiC hosts after identical electron irradiation (1×10^{18} cm^{-2} with 10 MeV) and annealing (1000 °C for 30 min) treatments. (b) Comparison of integrated PL intensities of divacancies in each host. All spectra were tested at 77 K.

To elucidate the formation mechanism, the defect evolution during irradiation and annealing processes was compared across hosts, as shown in Fig. 2. Two typical spectra ranges were selected. E_A peaks (*a*–*f*) are the production of electron irradiation and related to kinds of vacancies or interstitials.[36–39] V_{Si} are key precursors for divacancy formation, which is the characteristic deep-level defects for the semi-insulating property of HPSI 4H-SiC hosts.[40–42] For pristine hosts, no E_A peaks are detected in HPSI-1, n-type or p-type hosts, whereas E_A peak *e* is present in the epitaxial host and peaks *b*–*f* are detected in HPSI-2, as shown in Fig. 2(a). The types of E_A defects among hosts vary, even in different HPSI substrates. V_{Si} are clearly observed in HPSI-1 and HPSI-2, as shown in Fig. 2(b), consistent with their role in pinning the Fermi level of HPSI wafers.[43–46] However, the V_{Si} intensity of HPSI-1 is higher than that of HPSI-2, while it is not detected in other hosts. Therefore, their Fermi levels are different with different deep-level-defect systems.[47–49] After electron irradiation, E_A-related defects are prominently generated in HPSI and epitaxial hosts, while the signals are weak in the n-type host and not detected in the p-type host, as shown in Fig. 2(c). Meanwhile, V_{Si} were detected in all samples except the p-type host, as shown in Fig. 2(d). The irradiation-induced defects across hosts are similar, while their intensities vary with different host types. The yields of defects positively connected with the results in Fig. 1, as defects generated with electron irradiation are precursors for divacancies. After annealing, E_A peak *e* persists in all hosts except the p-type one, whereas the additional E_A peaks *b* and *c* remain only in HPSI-2. Meanwhile, the signals of V_{Si} are still detectable in HPSI and epitaxial hosts, as shown in Figs. 2(e) and 2(f). The annealing temperature exceeds the activation barrier of Frenkel pairs, interstitials (C_i, Si_i), and V_{Si}.[50,51] Consequently, defects migrate and interact during annealing, leading to changes in defect species and the formation of divacancies. The observed host preference for divacancy formation is therefore attributed to the differing concentrations of precursors generated by electron irradiation. Moreover, the distinct intrinsic defects of HPSI-1 are responsible for the specific production of PL5, which act as precursors in the kinetic evolution during annealing.

As PL5 is strongly connected with HPSI-1, the intrinsic defects were further compared between HPSI-1 and HPSI-2 with EPR spectra. In the pristine state, both hosts exhibit a single line with $g \approx 2.002$–2.003, as shown in Fig. 3(a). This peak is related to simple atomic defects such as vacancies, interstitials, and substitutional atoms.[52–54] A strong pair of lines with a large shift of *g*-factor in the HPSI-2 host is attributed to some unknown complex defects with low symmetry in prior reports.[55,56] Signals corresponding to simple atomic defects become dominant in both hosts after treatments, indicating the defect conversion during the process, as shown in Fig. 3(b). Three additional pairs of lines with large shifts of *g* factors in the HPSI-2 host appear, while no additional line was detected in HPSI-1. The EPR results confirm a marked difference in the intrinsic defect characteristics and their evolution paths between HPSI-1 and HPSI-2. In addition, complex defects in the host show no help for the generation of PL5.

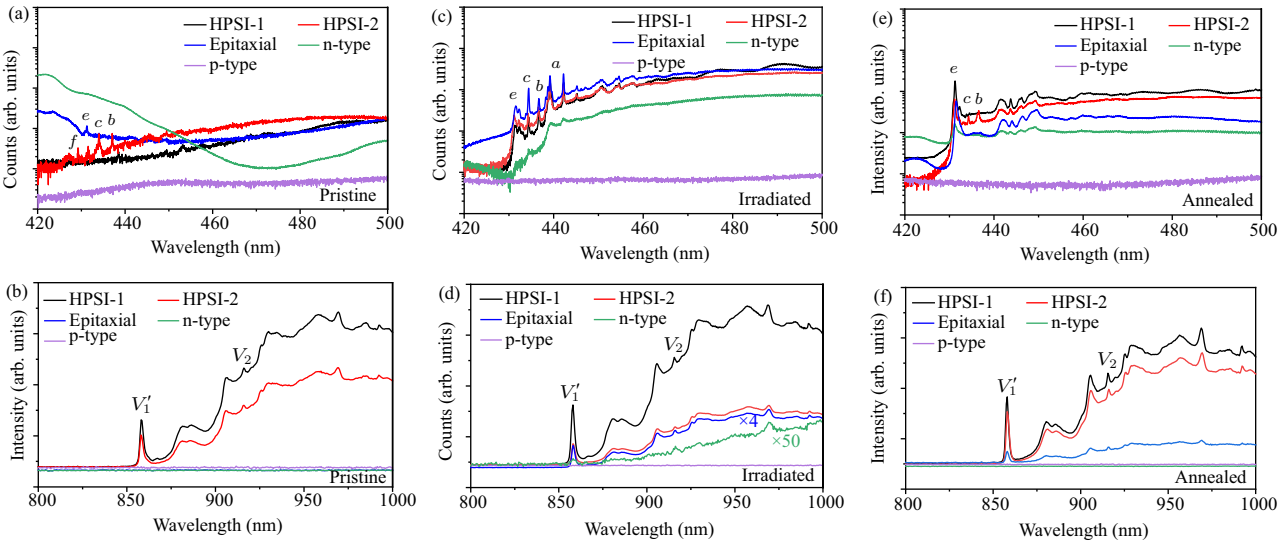


Fig. 2. PL spectra comparison (at 77 K) of different 4H-SiC hosts at stages of treatment, (a), (b) pristine wafers, (c), (d) after irradiation, (e), (f) after annealing.

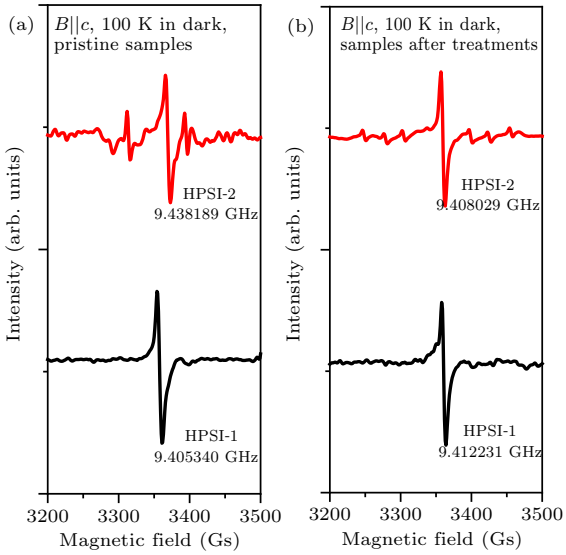


Fig. 3. EPR spectra of HPSI hosts (a) before and (b) after electron irradiation and annealing. Measurements were performed in the dark at 100 K with magnetic fields parallel to the *c*-axis of the samples.

Stacking faults can be generated or expanded with high-energy irradiation or high-temperature annealing.[57–61] Furthermore, the quantum well induced by stacking faults is theoretically predicted to produce PL5.[25] To clarify the connection between stacking faults and PL5, the crystal structure of the annealed HPSI-1 sample was analyzed with TEM, as shown in Fig. 4. Stacking faults show line contrasts in the TEM image.[62,63] No line contrast corresponding to stacking faults is observed in the bright-field image, as shown in Fig. 4(a). This suggests that the formation of PL5 is not necessarily connected with stacking faults in this work. Meanwhile, other defects such as dislocations or clusters are neither observed. The high-resolution TEM image confirms that the host crystal maintains the standard 4H stacking sequence (ABCB……) without local disruption in atomic arrangement, as shown in Fig. 4(b). This indicates that the possible processing damage has been repaired effectively. Therefore, electron irradiation followed by high-temperature annealing constitutes a mild process to generate divacancies. The existence of stacking faults is not necessary to generate PL5, which is beneficial for fabricating three-dimensional uniformly distributed PL5 ensembles.

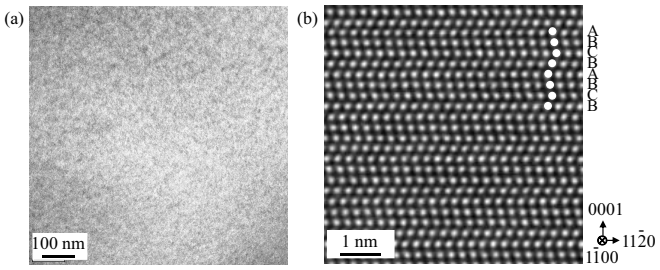


Fig. 4. (a) Bright-field TEM image and (b) high-resolution TEM image of annealed HPSI-1 sample along $[1\bar{1}00]$ direction

The depth distribution of divacancies was investigated by PL profiling along the *c*-axis. In HPSI-1, the intensities of PL1–PL5 are low near the surface and become stable in the bulk region, as shown in Fig. 5(a). In contrast, PL1–PL4 in HPSI-2 gradually decrease with increasing depth, as shown in Fig. 5(b). No signal of PL5 can be detected in HPSI-2, indicating that the formation of PL5 is not position-dependent. In the epitaxial host, the divacancy signals appear in the epilayer and become undetectable across the interface into the substrate, as shown in Fig. 5(c). This confirms the analysis of Fig. 1 that the heavily doped n-type substrate is inefficient to generate divacancy. The distinct divacancy distributions among the three hosts are governed by the spatial distribution of precursors V_{Si} (Figs. S4–S6), which vary with hosts.

To investigate the kinetic evolution, the PL intensities of divacancies with isochronal annealing were compared from 800 °C to 1300 °C. The intensity of each peak is calcu-

lated from the peak area with Gaussian fitting. The annealing range exceeds the recombination of Frenkel pairs and the dissociation of complex clusters, simplifying the kinetic analysis of divacancy.[64,65] The formation of divacancy PL1–PL4 reached the maximum at 1000 °C in HPSI-1, as shown in Fig. 6(a). This is consistent with a dominant pathway of divacancy formation with V_{Si} migrating.[66,67] The signals of V_{Si} kept decreasing with increasing annealing temperature, as shown in Fig. 6(b). However, the intensities of PL1–PL4 decline beyond 1000 °C and become weak at 1300 °C, indicating that the dissociation of divacancies becomes dominant. The injection of interstitials also plays a role in the decrease of divacancies.[68,69] Notably, PL5 is detected within the range of 1000–1200 °C, whose signals are low. This suggests that PL5 exhibits a high formation barrier and low stability. The variation characteristics of PL1–PL4 and V_{Si} in HPSI-2 are similar to those in HPSI-1, as shown in Figs. 6(c) and 6(d). The signal of PL5 was not detected over the annealing range. The annealing behavior of divacancies in the epitaxial host resembles that in HPSI hosts, except that the divacancy intensity maximum occurs at 900 °C, as shown in Figs. 6(e) and 6(f). This shift can be explained by a reduced activation energy of V_{Si}, which is tuned by the Fermi level.[70] The peak positions of PL1–PL5 are also deduced from the Gaussian fittings to confirm the accuracy of the PL analysis (Fig. S7). The similar kinetic profiles among hosts indicate that the precursors generated by electron irradiation play a major role in the fabrication of divacancies, which are highly consistent in Fig. 2. The isochronal annealing results indicate that the electron irradiation followed by annealing provides a general route to fabricate divacancy ensembles in various hosts. The migration of V_{Si} dominates the formation process of divacancies, which is tuned by the Fermi level, and leads to a preferred annealing temperature in different hosts. Although the PL5 ensemble forms simultaneously with PL1–PL4, its formation is restricted to a narrow kinetic window.

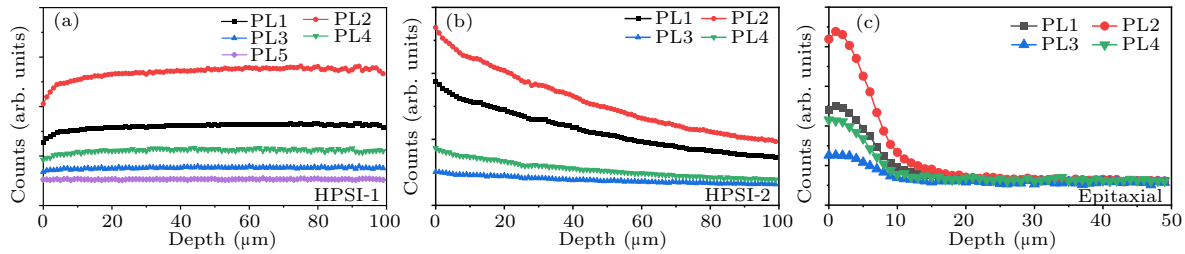


Fig. 5. Depth profiles of divacancy PL intensity along the *c*-axis in (a) HPSI-1, (b) HPSI-2, (c) epitaxial hosts tested with PL at 77 K.

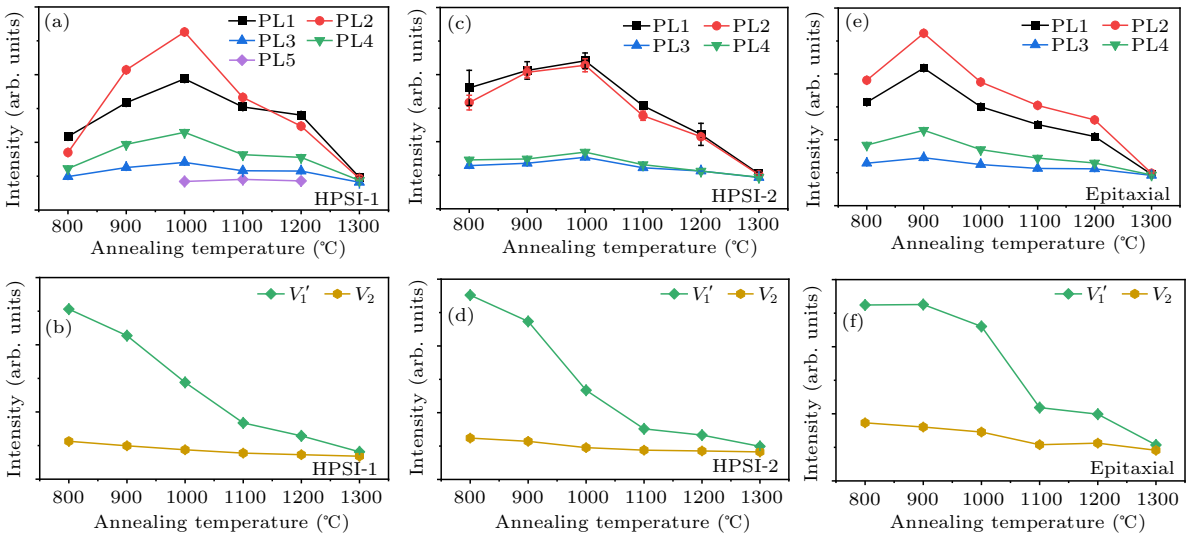


Fig. 6. Evolution of PL intensities for divacancies and V_{Si} during isochronal annealing in (a), (b) HPSI-1, (c), (d) HPSI-2, (e), (f) epitaxial hosts. The final temperature varied while the annealing steps were kept the same.

With an external magnetic field, the ODMR resonance of PL1 splits into a Zeeman doublet at room temperature both in HPSI-1 and HPSI-2, as shown in Fig. 7. The peak position accords well with former reports of as-grown samples.[71,72] Signals of PL2–PL4 are not detected, which is attributed to their poor room-temperature coherent properties.[24,72,73] The signal in the epitaxial host is beyond the limitation of the detector used in this work. With Gaussian fitting, the contrast (*C*) and full width at half maximum (FWHM) of PL1 were extracted. The contrast obtained from HPSI-1 is higher than that from HPSI-2, indicating a high concentration of activated color centers, which agrees with the PL spectra analysis. The FWHM of HPSI-1 is also better than that of HPSI-2. Results indicate that the high concentration of PL1 ensembles are success-

fully fabricated and are ready for practical quantum sensing at room temperature. With the specific symmetry characteristics of PL1, no additional process is needed to distinguish its signals from different axial orientations.[74] This feature makes the PL1 ensemble a promising candidate for vector measurements of multi-physical fields.

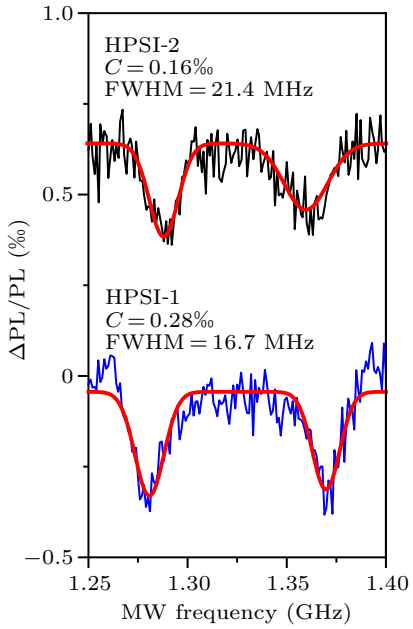


Fig. 7. Room-temperature ODMR spectra of PL1 ensemble in HPSI-1 and HPSI-2 hosts under external magnetic field (laser energy = 180 mW, microwave power = 10 dbm).

4. Conclusion

With a comparative study of divacancy formation across a series of hosts, several levels of formation preference have been identified. First, HPSI wafers are preferred for high concentrations of conventional divacancies PL1–PL4. The signal of divacancy is not detected in n- and p-type substrates in this work. The reason is the various generation efficiencies of precursors for divacancy across hosts. Therefore, the HPSI-type wafer is proved to be a valid candidate for the fabrication of divacancy ensembles. Second, PL1 and PL2 consistently dominate ensembles across types of hosts and different isochronal annealing temperatures, indicating a pronounced type selectivity in the fabrication process. In addition, the kinetic process of divacancy formation is tuned by the Fermi level of hosts. Third, the formation of PL5 exhibits host preference, which occurs only in one HPSI host with particularly intrinsic defects assisting the formation. The effect of complex defects has been ruled out. Finally, the PL1 ensembles are successfully applied to magnetic-field detection at room temperature, which is suitable for quantum measurements with the specific axial symmetry. With the analysis of the formation mechanism and experimental performance, this work advances divacancy ensembles in 4H-SiC towards the practical quantum-sensing applications.

Acknowledgements

This work is supported by the National Key Research and Development Program of China (Grant No. 2023YFF0718400), the Major Program of Natural Science Foundation of Zhejiang Province, China (Grant No. LD25A040001), and the National Natural Science Foundation of China (Grant No. 12302207), the "Pioneer" and "Leading Goose" R&D Program of Zhejiang Province, China (Grant Nos. 2025C01041 and 2025C2027).

References

[1] Oberg L, Weber C, Yang H H, Klesse W M, Reinke P, Corujeira Gallo S, Stacey A, Pakes C I and Doherty M W 2025 *Mater. Quantum Technol.* **5** 033001
[2] Yang Y, Lin S, Zhao J, Weng C, Lou L, Zhu W and Wang G 2025 *Chin. Phys. B* **34** 056102
[3] Castelletto S, Lew C T K, Lin W X and Xu J S 2024 *Rep. Prog. Phys.* **87** 014501
[4] Koehl W F, Buckley B B, Heremans F J, Calusine G and Awschalom D D 2011 *Nature* **479** 84
[5] Zhu M D, Yan L, Qin X, Zhang W Z, Lin Y and Du J 2023 *Chin. Phys. B* **32** 090702
[6] Tusun M, Rong X and Du J 2019 *Chin. Phys. B* **28** 024204
[7] Wolfowicz G, Whiteley S J and Awschalom D D 2018 *Proc. Natl. Acad. Sci. USA* **115** 7879
[8] Liu L, Wang J F, Liu X D, Xu H A, Cui J M, Li Q, Zhou J Y, Lin W X, He Z X, Xu W, Wei Y, Liu Z H, Wang P, Hao Z H, Ding J F, Li H O, Liu W, Li H, You L, Xu J S, Gregoryanz E, Li C F and Guo G C 2022 *Nano Lett.* **22** 9943
[9] Wang J F, Cui J M, Yan F F, Li Q, Cheng Z D, Liu Z H, Lin Z H, Xu J S, Li C F and Guo G C 2020 *Phys. Rev. B* **101** 064102
[10] Chen X, Luo Q Y, Guo P J, Zhou H J, Hu Q C, Wu H P, Shen X W, Cui R Y, Dong L, Wei T X, Xiao Y H, Li D, Lei L, Zhang X, Wang J F and Xiang G 2024 *Adv. Funct. Mater.* **35** 2413529
[11] Son N T, Umeda T, Isoya J, Gali A, Bockstedte M, Magnusson B, Ellison A, Morishita N, Ohshima T, Itoh H and Janzén E 2006 *Physica B* **376–377** 334
[12] Baranov P G, Il'in I V, Mokhov E N, Muzafarova M V, Orlinskii S B and Schmidt J 2005 *JETP Lett.* **82** 441
[13] Beste A, Taylor D E, Golter D A and Lai C W 2018 *Phys. Rev. B* **98** 214107
[14] Gordon L, Janotti A and Van de Walle C G 2015 *Phys. Rev. B* **92** 045208
[15] Falk A L, Klimov P V, Buckley B B, Ivády V, Abrikosov I A, Calusine G, Koehl W F, Gali Á and Awschalom D D 2014 *Phys. Rev. Lett.* **112** 187601
[16] Luo Q Y, Zhao S, Hu Q C, Quan W K, Zhu Z Q, Li J J and Wang J F 2023 *Nanoscale* **15** 8432
[17] Yan F F, Wang J F, Li Q, Cheng Z D, Cui J M, Liu W Z, Xu J S, Li C F, and Guo G C 2018 *Phys. Rev. Appl.* **10** 044042
[18] Falk A L, Buckley B B, Calusine G, Koehl W F, Dobrovitski V V, Politi A, Zorman C A, Feng P X L and Awschalom D D 2013 *Nat. Commun.* **4** 1819
[19] Bao T, Luo Q, Yi A, Liang B, Zhang Y, Hu H B, Lai S, Liu Z, Xiao S, Ou X, Zhou Y and Song Q 2025 *ACS Photonics* **12** 2988
[20] He Z X, Zhou J Y, Li Q, Lin W X, Liang R J, Wang J F, Wen X L, Hao Z H, Liu W, Ren S, Li H, You L X, Zhang R J, Zhang F, Tang J S, Xu J S, Li C F and Guo G C 2024 *Nat. Commun.* **15** 10146
[21] Zhou J Y, Li Q, Hao Z Y, Yan F F, Yang M, Wang J F, Lin W X, Liu Z H, Liu W, Li H, You L, Xu J S, Li C F and Guo G C 2021 *ACS Photonics* **8** 2384
[22] Zhou J Y, Li Q, Hao Z H, Lin W X, He Z X, Liang R J, Guo L, Li H, You L, Tang J S, Xu J S, Li C F and Guo G C 2023 *Nano Lett.* **23** 4334
[23] Christle D J, Falk A L, Andrich P, Klimov P V, Hassan J U, Son Nguyen T, Janzén E, Ohshima T and Awschalom D D 2015 *Nat. Mater.* **14** 160
[24] Li Q, Wang J F, Yan F F, Zhou J Y, Wang H F, Liu H, Guo L P, Zhou X, Gali A, Liu Z H, Wang Z Q, Sun K, Guo G P, Tang J S, Li H, You L X, Xu J S, Li C F and Guo G C 2022 *Natl. Sci. Rev.* **9** nwab122

[25] Ivady V, Davidsson J, Delegan N, Falk A L, Klimov P V, Whiteley S J, Hruszkewycz S O, Holt M V, Heremans F J, Son N T, Awschalom D D, Abrikosov I A and Gali A 2019 *Nat. Commun.* **10** 5607

[26] Son N T, Shafizadeh D, Ohshima T and Ivanov I G 2022 *J. Appl. Phys.* **132** 025703

[27] Bai R, Liu D, Chen S and Wu Y N 2025 *Phys. Rev. B* **111** 014106

[28] Hao Z H, He Z X, Maksimovic J, Katkus T, Xu J S, Juodkazis S, Li C F, Guo G C and Castelletto S 2025 *ACS Photonics* **12** 1552

[29] Campbell B and Mainwood A 2000 *Phys. Status Solidi A* **181** 99

[30] Chen X D, Yang C L, Gong M, Ge W K, Fung S, Beling C D, Wang J N, Lui M K and Ling C C 2004 *Phys. Rev. Lett.* **92** 125504

[31] Almutairi A F M, Partridge J G, Xu C, Cole I S and Holland A S 2022 *Appl. Phys. Lett.* **120** 014003

[32] Kimura T, Ahn J, Delegan N, Dibos A, Zhang J, Pingault B, Zhang C, Galli G, Awschalom D and Heremans F J 2025 *Appl. Phys. Lett.* **126** 164001

[33] Žalandauskas V, Silkinis R, Vines L, Razinkovas L and Bathen M E 2025 *npj Comput. Mater.* **11** 155

[34] Jin Y, Govoni M, Wolfowicz G, Sullivan S E, Heremans F J, Awschalom D D and Galli G 2021 *Phys. Rev. Mater.* **5** 084603

[35] Magnusson B, Son N T, Csóré A, Gällström A, Ohshima T, Gali A and Ivanov I G 2018 *Phys. Rev. B* **98** 195202

[36] Litrico G, Zimbone M, Baratta G, Marino A D M, Musumeci P and Calcagno L 2010 *Nucl. Iinstrum. Meth. B* **268** 2947

[37] Steeds J W, Evans G A, Danks L R, Furkert S, Voegeli W, Ismail M M and Carosella F 2002 *Diamond Relat. Mater.* **11** 1923

[38] Egilsson T, Henry A, Ivanov I G, Lindstrom J L and Janzen E 1999 *Phys. Rev. B* **59** 8008

[39] Knežević T, Hadžipašić A, Ohshima T, Makino T and Capan I 2022 *Appl. Phys. Lett.* **120** 252101

[40] Bathen M E, Galeckas A, Karsthof R, Delteil A, Sallet V, Kuznetsov A Y and Vines L 2021 *Phys. Rev. B* **104** 045120

[41] Nagy R, Widmann M, Niethammer M, Dasari D B R, Gerhardt I, Soykal Ö O, Radulaski M, Ohshima T, Vučković J, Son N T, Ivanov I G, Economou S E, Bonato C, Lee S Y and Wrachtrup J 2018 *Phys. Rev. Appl.* **9** 034022

[42] Janzén E, Gali A, Carlsson P, Gällström A, Magnusson B and Son N T 2009 *Physica B* **404** 4354

[43] Jiang S, Li Y, Chen Z, Zhu W, Wu Q, He H and Wang X 2022 *AIP Adv.* **12** 065311

[44] Janzén E, Son N T, Magnusson B and Ellison A 2006 *Microelectron. Eng.* **83** 130

[45] Chandrashekhar M V S, Chowdhury I, Kaminski P, Kozlowski R, Klein P B and Sudarshan T 2012 *Appl. Phys. Express* **5** 025502

[46] Gelczuk Ł, Dabrowska-Szata M, Sochacki M and Szmidt J 2011 *Solid State Phenom.* **178–179** 366

[47] Son N T, Carlsson P, ul Hassan J, Magnusson B and Janzén E 2007 *Phys. Rev. B* **75** 155204

[48] Kimoto T 2016 *Prog. Cryst. Growth Charact. Mater.* **62** 329

[49] Karsthof R, Bathen M E, Galeckas A and Vines L 2020 *Phys. Rev. B* **102** 184111

[50] Bockstedte M, Mattausch A and Pankratov O 2004 *Phys. Rev. B* **69** 235202

[51] Zheng M J, Swaminathan N, Morgan D and Szlufarska I 2013 *Phys. Rev. B* **88** 054105

[52] Mizuochi N, Yamasaki S, Takizawa H, Morishita N, Ohshima T, Itoh H and Isoya J 2002 *Phys. Rev. B* **66** 235202

[53] Isoya J, Umeda T, Mizuochi N, Son N T, Janzén E and Ohshima T 2008 *Phys. Status Solidi B* **245** 1298

[54] Jenny J R, Müller S G, Powell A, Tsvetkov V F, Hobgood H M, Glass R C and Carter C H 2002 *J. Electron. Mater.* **31** 366

[55] Carlsson P, Son N T, Gali A, Isoya J, Morishita N, Ohshima T, Magnusson B and Janzén E 2010 *Phys. Rev. B* **82** 235203

[56] Gerstmann U, Seitsonen A P, Ceresoli D, Mauri F, von Bardeleben H J, Cantin J L and Garcia Lopez J 2010 *Phys. Rev. B* **81** 195208

[57] Lin Y R, Ho C Y, Hsieh C Y, Chang M T, Lo S C, Chen F R and Kai J J 2014 *Appl. Phys. Lett.* **104** 121909

[58] Liu C and Szlufarska I 2018 *J. Nucl. Mater.* **509** 392

[59] Sen H S, Daghbouj N, Li B S, AlMotasem A T, Ge F F, Zhang L, Callisti M and Polcar T 2023 *Acta Mater.* **256** 119129

[60] Parish C M, Koyanagi T, Kondo S and Katoh Y 2017 *Sci. Rep.* **7** 1198

[61] Yakimov E B, Yakimov E E, Orlov V I and Gogova D 2018 *Superlattices Microstruct.* **120** 7

[62] Asafuji R and Hijikata Y 2018 *Mater. Res. Express* **5** 015903

[63] Orlov V I, Regula G and Yakimov E B 2017 *Acta Mater.* **139** 155

[64] Lucas G and Pizzagalli L 2007 *J. Phys. Condens. Matter* **19** 086208

[65] Kuate Defo R, Zhang X, Bracher D, Kim G, Hu E and Kaxiras E 2018 *Phys. Rev. B* **98** 104103

[66] Lee E M Y, Yu A, de Pablo J J and Galli G 2021 *Nat. Commun.* **12** 6325

[67] Galeckas A, Karsthof R, Gana K, Kok A, Bathen M E, Vines L and Kuznetsov A 2022 *Phys. Status Solidi A* **220** 2200449

[68] Zhang R, Zhang M, Zhang G, Chen Y, Liu J, Tian Z, Yu Y, Zhao P, Cai J, Chen X, Lin D, Wu S, Zhang Y, Xu X, Hong R and Zhang F 2025 *Chin. Phys. B* **34** 067201

[69] Zolnai Z, Son N T, Hallin C and Janzén E 2004 *J. Appl. Phys.* **96** 2406

[70] Zhang C, Gygi F and Galli G 2023 *Nat. Commun.* **14** 5985

[71] Wang J F, Zhou J Y, Li Q, Yan F F, Yang M, Lin W X, Hao Z Y, Li Z P, Liu Z H, Liu W, Sun K, Wei Y, Tang J S, Xu J S, Li C F and Guo G C 2021 *Photonics Res.* **9** 1752

[72] Shafizadeh D, Son N T, Abrikosov I A and Ivanov I G 2025 *Phys. Rev. B* **111** 165201

[73] Toyli D M, Christle D J, Alkauskas A, Buckley B B, Van de Walle C G and Awschalom D D 2012 *Phys. Rev. X* **2** 031001

[74] Wang Y, Zhang R, Yang Y, Wu Q, Yu Z and Chen B 2023 *Chin. Phys. B* **32** 070301